RSC Advances

ROYAL SOCIETY OF CHEMISTRY

www.rsc.org/advances

Magnetically separable palladium nanoclusters supported iron based metal-organic frameworks (MIL-88B) catalyst in efficient hydrogenation reaction

Dewan Azharul Islam and Himadri Acharya

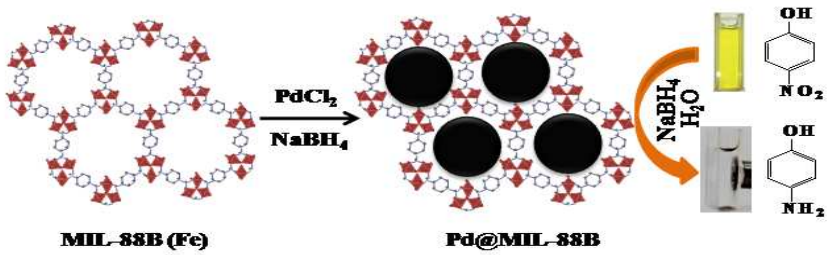

Magnetically separable palladium nanoclusters (Pd NCs) supported iron based metal-organic framework, Pd@MIL-88B catalyst for enhanced catalytic activity towards the reduction of 4-nitrophenol.

RSC Advances

RSCPublishing

ARTICLE

Magnetically separable palladium nanoclusters supported iron based metal-organic frameworks (MIL-88B) catalyst in efficient hydrogenation reaction

Cite this: DOI: 10.1039/x0xx00000x

Received 00th January 2012,
Accepted 00th January 2012

DOI: 10.1039/x0xx00000x

www.rsc.org/

D. A. Islam and H. Acharya*

A facile process to fabricate magnetically separable palladium nanoclusters (Pd NCs) supported iron based metal-organic framework, Pd@MIL-88B catalyst is reported. Highly active Pd NCs are obtained by simple in situ chemical reduction of immobilized metal salts within the porous MIL-88B. Structure and morphology analysis of the Pd@MIL-88B catalyst is characterized by X-ray diffraction (XRD), and transmission electron microscopy (TEM). The Pd@MIL-88B exhibit excellent catalytic activity towards the reduction of 4-nitrophenol completed in only 15 s at room temperature, even when the Pd content was 2.7 wt%. Moreover, the catalyst can be reused several times with significant recycling stabilities on magnetic separation.

Introduction

Transition metal nanostructures have attracted considerable attention to the researchers because of their widespread applications in electronics, photonics, catalysis, sensors, storage and biomedicine.[1-6] Among the various metal nanostructures, palladium nanostructures have gained huge attention over the past decades for their unique catalytic properties for different organic reactions in the chemical and pharmaceutical industries, including carbon–carbon cross-coupling and hydrogenation reactions, etc.[7-9] They are also good candidates as electrocatalysts for fuel cells and sensors.[10-12] Recently, Pd nanoclusters (Pd NCs) are of significant interest because they provide high surface-to-volume ratio and very active surface atoms available for the catalytic applications.[13-15] Because of their high surface energies and large surface areas these bare Pd NCs with small size easily aggregate into larger nanoparticles or bulk materials which are responsible for the decrease of their intrinsic catalytic activities. Therefore, stabilizers and supporting materials such as polymers, surfactants and colloids are often used to prevent the aggregation of NCs during reactions.[16-18] The stabilizers or capping agent may be responsible to limit the catalytic activities due to the surface contamination of the NCs. In this regard, the use of porous hybrid materials as support for NCs immobilization facilitate the generations of specific surfactant-free active sites with the advantages of control growth of well-distributed nanostructures in confined cavities and reduce the aggregation. Although many porous materials such as zeolites, silicas, and other porous inorganic/organic matrixes have been broadly used for producing metal nanostructures within their confined pores.[19,20] Metal organic frameworks (MOFs) are a particular class of multifunctional porous hybrid materials that support for metal NCs immobilization due to their tunable framework structures with specific pore sizes, shapes, and functionalities and electronic interaction between the metal NCs and organic linkers, which is promising for controlling the limited growth of metal NCs in their well-defined cavities and produce highly active monodispersed metal NCs.[21-25] Therefore, the use of highly porous MOFs as supports is a promising strategy for the preparation of well- distributed metal NCs that improve the chemical and thermal stability and enhance the catalytic activity of functioned materials. Encapsulation of metal NPs inside the pores of MOFs is an effective method[26-28] for improving heterogenous catalysis in comparison to other porous materials such as mesoporous carbon, silicas, due to their high surface area and well-defined cavities.[29,30] Although various metal based catalytic systems have been reported, that exhibits excellent catalytic properties, for example, the Au@Carbon[31] core-shell that catalyze for the reduction of 4-nitro phenol (4-NP) to 4- amino phenol (4-AP). But it is still remains challenge to synthesis of metal NPs encapsulated MOFs catalyst that exhibits further improve the reusable heterogeneous catalytic activities for the reduction of aromatic nitro compounds.

Herein, we report a facile solution impregnation method for the synthesis of highly active reusable magnetically separable Pd NCs supported iron based MOFs, Pd@MIL-88B catalyst by a

facile solution impregnation method. The Pd NCs were grown in the 3D porous structure of iron based MIL-88B by a simple solution impregnation and $NaBH_4$ reduction method (Fig. 1). MIL-88B provides large pores, high surface area and excellent chemical and thermal stability for the fabrication of size controlled monodisperse Pd NCs. The Pd@MIL-88B exhibits excellent catalytic activity for the reduction of 4-NP to 4-AP at ambient condition. It has been demonstrated that the reduction could be complete even within 15s when 2.7% of Pd NCs used. Notably, this new material offers most effective catalytic performance for the reduction of 4-NP. MIL-88B as a novel magnetically separable host is also an interesting in efficient separation of heterogeneous catalysts from solutions upon reaction completion by applying a simple magnet with good recycling stability in aqueous solution.

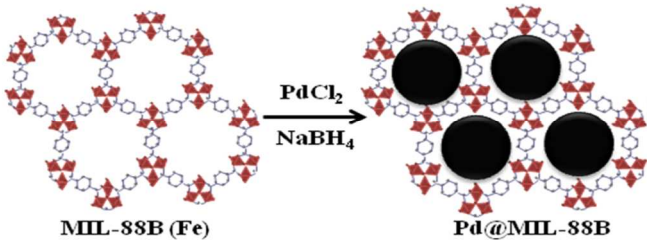

Fig. 1 Schematic representation of the fabrication of Pd nanoclusters supported iron based metal organic framework MIL-88B.

Experimental Section

Materials

Ferric chloride hexahydrate ($FeCl_3 .6H_2O$), terephthalic acid, palladium chloride ($PdCl_2$), sodium borohydride ($NaBH_4$) and poly vinyl pyrrolidone (PVP) were purchased from Sigma-Aldrich Chemical Co. dimethyl formamide (DMF), chloroform ($CHCl_3$), methanol and ethanol are acquired from Sisco Research Laboratories pvt. Ltd. All the chemicals and solvents are ACS reagent grade. Deionized water was used in all the experimental processes.

Preparation of MIL-88B(Fe)

Three dimensional MIL-88B(Fe) was synthesized by sovothermal reaction of 1:1 mixture of $FeCl_3.6H_2O$ (1.35 g, 5 mmol) and terephthalic acid (0.83 g, 5 mmol) in DMF at 130 °C. Then, the brown solid was recovered by filtration and repeated washing with deionised water to remove the unreacted part. The product was then collected and dried at room temperature in desiccators for 24 hours. MIL-88B was soaked and activated with chloroform by immersing for 24 hours. The product was then collected and dried at room temperature in desiccators for 24 hours.

Preparation of Pd@MIL-88B(Fe)

Pd nanoclusters supported MIL-88(Fe) was synthesized by a simple chemical reduction of impregnated palladium salts in the porous MIL-88B framework. Methanolic solution of H_2PdCl_4 (0.026g of $PdCl_2$ and 50 µL of conc. HCl in 20 ml methanol) was impregnated in MIL-88B (0.4 g) for 3 hours at ambient condition. The mixture was then evaporated to $1/3^{rd}$ under reduced pressure at room temperature. The mixture was then filtered, washed and dried at ambient temperature for 24 hours. The impregnated mixture was taken in ice cooled (0-3 ^oC) 10 ml methanolic solution and subsequently $NaBH_4$ solution (0.015 g in methanol) added under vigorous stirring for 45 mins, where impregnated Pd (II) salt is reduced to Pd(0) in the pores of MIL-88B and generating the Pd NCs. The colour of the reaction mixture changed from brown to black and the product so form was collected by centrifugation.

Dissolution of the host framework in Pd@MIL-88B(Fe)

Pd@MIL-88B composites were dissolved in a solution of ethylenediaminetetraacetic acid disodium salt (Na_2EDTA, 0.1N) to remove the host MIL-88B framework. 100 mg of Pd@MIL-88B was dissolved in 500mL 0.1 N Na_2EDTA solutions by sonicating the mixture for 10 mins and kept the mixture for 12 hours for complete removal of host matrix and the black coloured Pd nanoparticles were collected by centrifugation and washed 3-4 times with distilled water.

Preparation of PVP stabilized Pd nanoparticles

H_2PdCl_4 aqueous solution (2.0 mM) was prepared by mixing 17.4 mg of $PdCl_2$ (0.1 mmol), 1.0 mL of 0.2 M HCl, in 49 mL of distilled water. A mixture of 15 mL of 2.0 mM H_2PdCl_4 aqueous solution and 20 mL ethanol containing 20 mg PVP was stirred for 1 hour. Then 8.5 mg (0.225 mmol) $NaBH_4$ (0.1 M, 2 mL) was added to reaction mixture under vigorous stirring at ice cooled (0-3^oC) condition for 1 hour to obtained dark colloidial dispersion of Pd nanoparticles.

Catalytic study

The catalytic performance of the Pd@MIL-88B was tested by employing the reduction of 4-NP to 4-AP in presence of excess $NaBH_4$ aqueous solution at room temperature as a model reaction. In this study, first aqueous solution of $NaBH_4$ (0.1M, 0.7 mL) was added to the aqueous mixture of 4-NP (0.2 mM, 3 mL) contained in a glass vessel. After that, a given amount of Pd@MIL-88B nanocomposites were added to it. Immediately after addition of Pd@MIL-88B nanocomposites, the reaction progress was monitored by UV-visible spectra of the mixture to evaluate the catalytic activity and stability of the catalysts.

Characterization

Powder X-ray diffraction (XRD) was carried out with an X-ray diffractometer of BRUKER-D8 advance X-ray diffractrometer with Cu-K∞ radiation at λ = 1.5406 Å passed through a 0.04 rad Soller slit, a 1.0 mm fixed mask with 1.0° divergence slit, and a 0.2° anti-scatter slit. Transmission electron microscopy (TEM) and bright-field high resolution transmission electron microscopy (HRTEM) images were recorded on a JEOL, JEM-2100 transmission electron microscope with an accelerating voltage of 200 kV. TEM samples were prepared by drop casting from a dilute dispersion in methanol on carbon coated Cu-grid with 200 mesh sizes. The samples were dried overnight in air before characterization. FTIR spectra were recorded on a PERKIN-ELMER L 120-000A spectrometer (λ_{max} in cm^{-1}) on KBr pellets in the range 4000-400 cm^{-1}. UV-visible Spectra was recorded using JASCO V-670 spectrophotometer with 1 nm data interval in the range of 200 nm – 800 nm.

Results and Discussion

X ray diffraction (XRD) studies

The PXRD patterns of the synthesized MIL-88B and Pd@MIL-88B were shown in Fig. 2. Prominent reflections of the MIL-88B isolated from chloroform at 2θ value of 9.25°, 9.77° and 18.55° could be indexed to the (101), (002) and (202) planes of the hexagonal space group ($P\bar{6}2c$) of pure MIL-88B(Fe) phases. MIL-88B stabilizes the structure in its partially open form through weak van der Waals, π-π, and CH-π interactions of

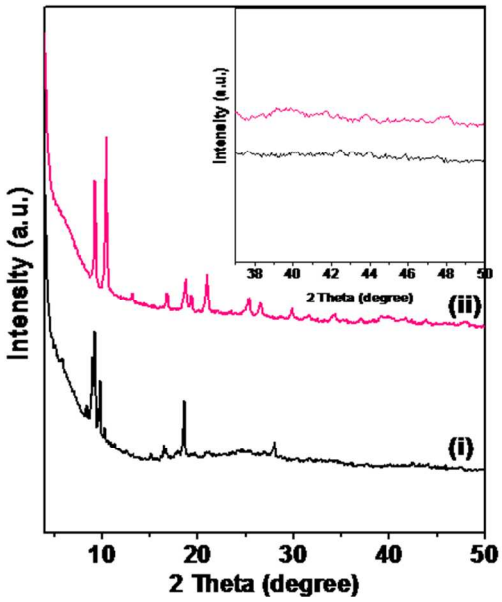

Fig. 2 Powder XRD patterns of the as prepared iron based (i) MIL-88B and (ii) Pd@MIL88B.

terephthalate linker. The PXRD pattern of Pd supported MIL-88B does not indicate any significant variations of the lattices. The overall reflection intensities of Pd@MIL-88B retains with respect to the parent MIL-88B, presumably suggest the Pd incorporation occurred with no apparent loss in the crystallinity. It is noteworthy that, the intensities of the prominent reflections at 9.25° and 10.45° of Pd@MIL-88B are inverted compared to the MIL-88B, which also suggests the presence of Pd NPs in the framework.[32] Simultaneously, the lattice shrinkage may occurs along the *a* axis of bipyramidal cages compared to the *c* axis breathing along (001) tunnels. This is due to the strong OH---O hydrogen bond interaction of polar solvent with inorganic carboxylate trimers of Fe(III) octahedral.[33] Moreover, PXRD pattern of Pd@MIL-88B exhibit a very broad and low intensity reflection at 39.0-40.0° 2θ which can be attributed to the (111) reflections of Pd nanoparticles in a size regime below 1 nm.[34,35] However other reflections of Pd NCs were not detected in the diffractometer probably attributed to the very small sizes and low degree of Pd NCs loading within the MIL-88B framework.

UV-visible studies

The UV-visible spectra in Fig. 3 suggest the presence of coordination mode in MIL-88B characteristic peaks of Pd NCs. The ligand-to-metal charge transfer transition occurs at 240 nm implies the bonding of carboxylate oxygen to Fe^{3+} metal. This band diminishes and red shifts by ~ 4nm on Pd NCs formation. The absorption band at 300–500 nm which is characteristic of the transition [$^6A_{1g}$ => $^4A_{1g}$ +^4E_g(G)] of Fe^{3+} is increased and also red shifted on Pd NCs formation.

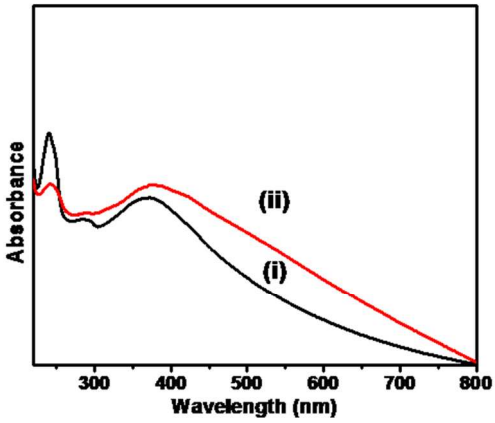

Fig. 3 UV-Vis spectra of (i) MIL-88B(Fe) and (ii) Pd@MIL-88B.

.

Transmission electron microscopy (TEM)

The morphology of the Pd NCs supported MIL-88B was further demonstrated by transmission electron microscopy analysis. The TEM image in Fig. 4(a) shows the well dispersed Pd NCs grown on the porous MIL-88B matrix. The typical needle shaped crystal of MIL-88B with dimension in the range of 200-

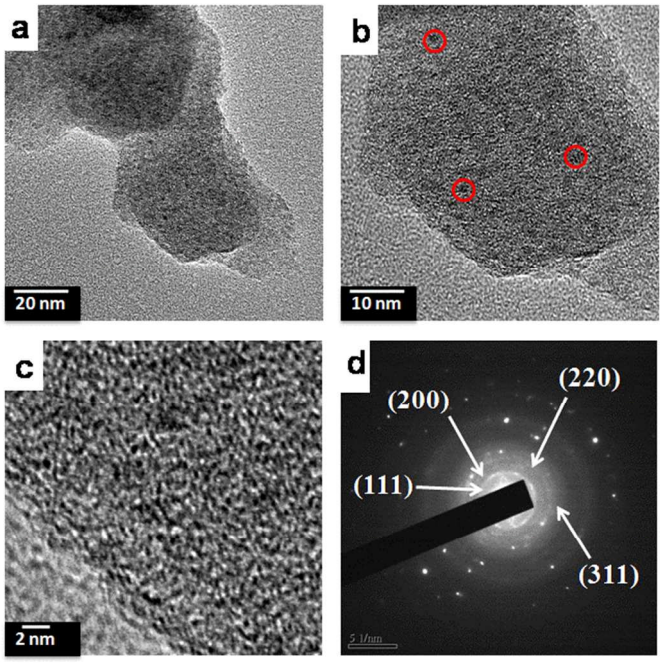

Fig. 4 (a) TEM images of Pd nanoclusters supported porous MIL-88B(Fe) frameworks. (b) high magnification image showing highly dispersed nanoclusters in MIL-88B(Fe) with local aggregation. (c) HRTEM bright field image of Pd NCs in the MIL-88B framework supports, the dark spots corresponds to the Pd NCs. (d) SAED patterns of polycrystalline Pd in MIL-88B.

400 nm was formed (Fig. S1, ESI†). The high-magnification images in Fig. 4(b) shows the presence of few localised ultrasmall nanoclusters aggregates with ~ 3 nm in diameter. The HRTEM image with lattice spacing of 0.229 nm is typical of a Pd (111) facets, consistent with the reported face centered cubic (fcc) Pd structure (Fig. S2, ESI†). To increase the contrast of the Pd NCs against the MOF support, we also measured bright field HRTEM images of Pd@MIL-88B as shown in Fig. 4(c). We could find that the particle has a diameter less than 1 nm, which indicates that the formed Pd NCs are well-dispersed on the MIL-88B. The selected area electron diffraction pattern (SAED) pattern in Fig. 4(d) shows the ring pattern typical of polycrystalline cubic Pd NCs.

Fourier transforms infrared spectroscopy (FTIR)

FTIR spectra shown in Fig. 5 further support the inclusion of Pd NCs on MIL-88B framework structures. The peaks in which the spectra of MIL-88B centered at about 3142 cm^{-1} and 3196 cm^{-1} corresponds to symmetric and anti symmetric O-H stretching vibration of coordinated water and band at 2991cm^{-1}, 1745 cm^{-1}, 1601 cm^{-1}, 1387 cm^{-1} and 532 cm^{-1} corresponds to C-H, C=O, aromatic C=C, OCO and Fe-O stretching vibration. But For Pd@MIL-88B, the O-H symmetric and asymmetric band appears at around 3144 cm^{-1} and 3192 cm^{-1}. The C=O stretching vibration shifted to 1747 cm^{-1} may be due to the

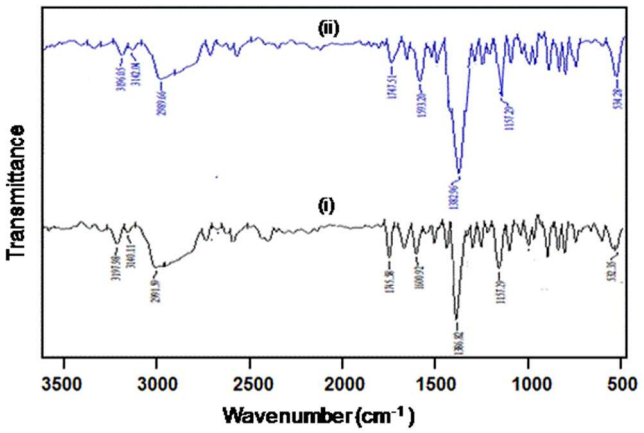

Fig. 5 FTIR spectra of (i) MIL-88B and (ii) Pd@MIL-88B.

dipole-induced dipole interaction between MIL-88B and Pd NCs. The aromatic C=C stretching vibration and OCO band shifted to 1593 cm^{-1} and 1383 cm^{-1} reveals the presence of Pd NCs in the porous surface of the MIL-88B.

Catalytic activity on hydrogenation

The catalytic performance of Pd NCs supported MIL-88B was evaluated for the reduction of 4-NP by $NaBH_4$ to 4-AP and the results are shown in Fig. 6. The reaction can easily be monitored by its visual colour change with catalyst and reduction kinetics was investigated by UV-visible absorption spectroscopy. The aqueous mixture of 4- NP (0.2 mM, 3 mL) and excess $NaBH_4$ (0.1M) appears bright yellow colour due to

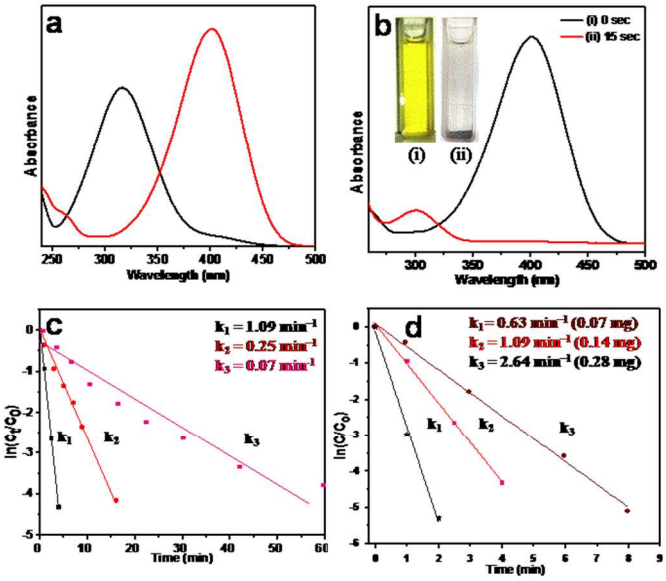

Fig. 6 (a) The UV-vis absorption spectra of 4-nitrophenol and 4-nitrophenolate (b) Catalytic reduction of 4-nitrophenol in presence of 1 mg Pd@MIL-88B catalyst. Inset of the figure shows the color change from yellow to colorless only in 15 s. (c) The rates constant plots of hydrogenation reactions determined from the different catalyst, Pd@MIL-88B (k_1), Pd NPs after isolation in PVP by dissolution of MIL-88B (k_2) and bare Pd NPs isolated in water by dissolution of MIL-88B (k_3) . (d) Effect of different wt% of catalyst in the rate constant of hydrogenation reaction.

the formation of 4- nitrophenolate as featured by a characteristic UV-visible peak at 400 nm (Fig. 6a). The reduction of 4-NP is attributed to the large potential difference between $E^0_{4\text{-NP/4-AP}} = -0.76$ V and $E^0_{H3BO3/BH4-} = -1.33$ V. The bright yellow solution gradually faded as the reaction proceeded after addition of the catalyst, indicating thereby the formation of 4-AP (Fig. 6b). The absorption peak of 4-nitrophenolate decreases with the concomitant increase in the absorption peak at 300 nm for 4-AP. It is noteworthy that the reduction was completed only in 15 s at room temperature, even when the Pd content of the catalyst was 2.7 wt%. The UV-visible spectra shows an isobestic point around 318 nm, implies that the 4-AP as a sole product. In the reaction mixture, the concentration of the BH_4^- was much higher and assumed to remain constant compare to the concentration of 4-NP. Since, the reaction appears independent of the concentration of BH_4^-, the rates of the reaction are assumed to be pseudo-first order kinetics with regard to 4-NP. The plot of $\ln(C_t/C_0)$ vs time shows a straight line with a negative slope to evaluate the rate constant. The rate constant k value was calculated to be 1.09 min^{-1} with 0.14 mg (Fig. 6c) of catalyst at room temperature and the catalyst activity parameter (ratio of rate constant to amount of catalyst added, i.e., $k_a = k/m$) was found to be 129.76 $s^{-1}g^{-1}$, which is much higher than the so far other reported catalyst (Table 1).

Table 1 Comparison of the rate constant and catalyst activity parameter of different types of catalysts.

Types of catalysts	Catalyst (mg)	Rate constant k,(min^{-1})	Catalyst activity parameter, k_a=k/m ($s^{-1}g^{-1}$)	Ref.
Pd@MIL-88	0.14	1.09	129.76	This work
Pd nanoparticles	0.14	0.25	29.76	This work
Mesoporous Palladium Leaves (MPL)	0.25	0.49	32.67	38
Au@Ag/ZIF-8	3.46	0.30	1.45	39
Ni/graphene	3	0.702	3.9	40

To demonstrate the high catalytic activity of Pd@MIL-88B, isolation of supported NPs was performed by complete dissolution of host MIL-88B framework in tetrasodium ethylenediaminetetraacetate (Na-EDTA; pKb = 3.8) solutions with and without PVP as stabilizing agent (Fig. S3 and S4, ESI†). The catalytic performance of PVP stabilized 3 nm Pd NPs separated from the MIL-88B shows the slower reduction process than Pd@MIL-88. The rate constant value of PVP stabilized Pd NPs catalysts was calculated to be k = 0.25 min^{-1} under the same reaction conditions. The bare Pd NPs isolated from MIL-88B exhibit much slower catalytic activity with rate constant k = 0.07 min^{-1} (Fig. S5, ESI†). Therefore the observed enhanced catalytic performance of Pd@MIL-88B is possibly due to the higher dispersion and accessibility of active Pd NCs sites. The high surface area of ultrasmall nanoclusters in the MIL-88B and low nanoclusters-host interaction effectively increases the hydrogenation reactions. At the same time, the framework structure of the MIL-88B prevents the aggregation of Pd NCs and facilitate the absorption of 4-NP on the surface.[36,37] The reduction of 4-NP was also carried out with varying the catalyst amount (0.07 mg, 0.14 mg and 0.28 mg), which reveals that the reaction rate increases with increasing the catalyst dose (Fig. 6d).

We explored the catalytic recyclability of Pd@MIL-88B by performing the same reduction reaction with same catalyst for six successive cycles. The catalyst was repeatedly recovered by centrifugation and washing. The conversion was nearly 100% within a reaction period of 15 s for 2.7 wt% Pd content in 1 mg catalyst. The rate constant values were almost remaining same up revealing the good stability of the catalyst. The reuse of the Pd@MIL-88B catalyst after magnetic isolation and separation upon reaction completion was also studied for several cycles. Results displayed in Fig. 7 confirm that the magnetically separable Pd NCs catalyst could be recycled and reused without any appreciable loss of its initial catalytic activity. The recycle stability of Pd@MIL-88B was even found to be > 90% after six times studied by repeating the hydrogenation of 4-NP. The UV-visible study of the reused catalyst also does not indicate any apparent changes in the absorption spectra (Fig. S6, ESI†). The inset figures indicate that the MIL-88B as a novel magnetically separable host allows a facile separation of the Pd NCs catalyst from the reaction mixture by applying a simple magnet, providing reusability in the designed systems for successive reaction runs.

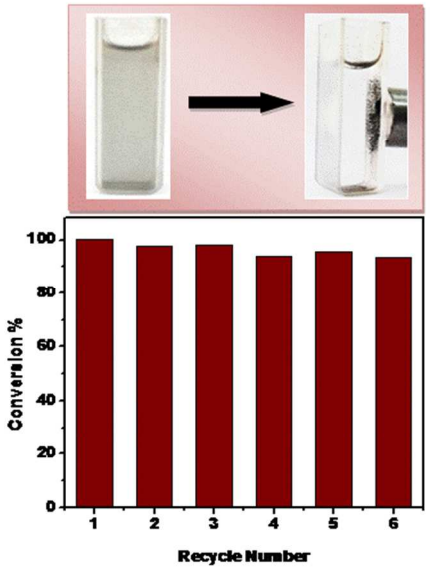

Fig. 7 Catalytic stability of Pd@MIL-88B with successive reuse cycles. Magnetic separation in the inset of the image.

Conclusions

In summary, we have synthesized magnetically separable well dispersed Pd nanoclusters supported MIL-88B by a facile solution impregnation method. MIL-88B acts as a support to control the size and monodispersity of Pd nanoclusters within the metal organic framework. The resultant Pd@MIL-88B possessed excellent catalytic activity for the reduction of 4-nitrophenol to 4-aminophenol in aqueous medium at ambient temperature. MIL-88B plays crucial role to enhance the catalytic activity of Pd nanoparticles via synergistic adsorption and electron transfer effect. The combination of highly efficient catalytic activity, good stability and recyclability makes Pd@MIL-88B a potential material for practical application on hydrogenation of aromatic nitro compounds.

Acknowledgements

The authors acknowledge the Department of Science and Technology (DST) and University Grants Commission (UGC), India for the financial support.

References

1 H. Wu, L. B. Hu, M. W. Rowell, D. Kong, J. J. Cha, J. R. McDonough, J. Zhu, Y. Yang, M. D. McGehee and Y. Cui, *Nano Lett*., 2010, **10**, 4242-4248.

2 X. F. Wu, H. Neumann and M. Beller, *Chem. Rev.,* 2013, **113**, 1–35.

3 S. Hu and X. Wang, *Chem. Soc. Rev.,* 2013, **42**, 5577-5592

4 D. A. Islam, D. Borah and H. Acharya, *RSC Adv*., 2015, **5**, 13239–13245

5 Y. Pak, S. M. Kim, H. Jeong, C. G. Kang, J. S. Park, H. Song, R. Lee, N. Myoung, B.H. Lee, S. Seo, J. T. Kim and G. Y. Jung, *ACS Appl. Mater. Interfaces.,* 2014, **6**, 13293–13298.

6 S. E. Allen, R. R. Walvoord, R. P. Salinas and M. C. Kozlowski, *Chem. Rev*., 2013, **113**, 6234–6458.

7 G. Collins, M. Blömker, M. Osiak, J. D. Holmes, M. Bredol and C. O'Dwyer, *Chem. Mater.,* 2013, **25**, 4312–4320.

8 Y. Wu, M. Wen, Q. Wu and H. Fang, *J. Phys. Chem. C.,* 2014, **118**, 6307–6313.

9 A. Cwik, Z. Hell and F. Figueras, *Org. Biomol. Chem*., 2005, **3**, 4307-4309.

10 J. Yang, Y. Xie, R. Wang, B. Jiang, C. Tian, G. Mu, J. Yin, B. Wang and H. Fu, *ACS Appl. Mater. Interfaces*., 2013, **5**, 6571–6579.

11 D. Wen, S. J. Guo, S. J. Dong and E. K. Wang, *Biosens. Bioelectron*., 2010, **26**, 1056-1061.

12 B. Fang, J. H. Kim, M. Kim and J.-S. Yu, *Chem. Mater.,* 2009, **21**, 789–796.

13 J. Wang, L. Hu, X. Cao, J. Lu, X. Li and H. Gu, *RSC Adv*., 2013, **3**, 4899-4902.

14 M. Hyotanishi, Y. Isomura, H. Yamamoto, H. Kawasaki and Y. Obora, *Chem. Commun*., 2011, **47**, 5750–5752.

15 Y. Wu, D. Wang, P. Zhao, Z. Niu, Q. Peng and Y. Li, *Inorg. Chem.,* 2011, **50**, 2046–2048.

16 H. Acharya, J. Sung, B. H. Sohn, D. H. Kim, K. Tamada and C. Park, *Chem. Mater.,* 2009, **21**, 4248-4255.

17 N. Sahiner, A. Kaynak and S. Butun, *J.Non-Cryst. Solids*., 2012, **358**, 758.

18 H. Acharya, J. Sung, T. H. Kim, D. H. Kim and C. Park, *Chemistry-A European Journal*. 2012, **18**, 14695-14701.

19 R. J. White, R. Luque, V. L. Budarin, J. H. Clark and D. J. Macquarrie, *Chem. Soc. Rev*., 2009, **38**, 481.

20 Z. R. Herm, E. D. Bloch and J. R. Long, *Chem. Mater*., 2014, **26**, 323–338.

21 G. T. Vuong, M. H. Pham and T. O. Do, *Dalton Trans*., 2013, **42**, 550-557.

22 N. A. Ramsahye, T. K. Trung, L. Scott, F. Nouar, T. Devic, P. Horcajada, E. Magnier, O. David, C. Serre and P. Trens, *Chem. Mater*., 2013, **25**, 479–488.

23 A. C. McKinlay, J. F. Eubank, S. Wuttke, B. Xiao, P. S. Wheatley, P. Bazin, M. Lavalley, J.-C. Daturi, A. Vimont, G. D. Weireld, P. Horcajada, C. Serre and R. E. Morris, *Chem. Mater*., 2013, **25**, 1592–1599.

24 A. Dhakshinamoorthy and H. Garcia, *Chem. Soc. Rev*., 2012, **41**, 5262.

25 H. R. Moon, D. W. Limb and M. P. Suh, *Chem. Soc. Rev*., 2013, **42**, 1807.

26 J. J. Alcaniz, J. Gascon and F. Kapteijin, *J. Mater. Chem*., 2012, **22**, 10102.

27 M. Meilikhov, K. Yusenko, D. Esken, S. Turner, G. V. Tendeloo and R. A. Fischer, *Eur. J. Inorg. Chem.*, 2010, **24**, 3701.

28 A. Aijaz, A. Karkamkar, Y. J. Choi, N. Tsumori, E. Ronnebro, T. Autrey, H. Shioyama and Q. Xu, *J. Am. Chem. Soc*., 2012, **134**, 13926.

29 J. Zeng, C. Francia, C. Gerbaldi, M. A. Dumitrescu, S. Specchia and P. Spinelli, *J. Solid State Electrochem*., 2012, **16**, 3087.

30 L. Wang, H. Wang, P. Hapala, L.F. Zhu, L. M. Ren, X. J. Meng, J. P. Lewis and F. S. Xiao, *J. Catal.*, 2011, **281**, 30.

31 R. Liu, *Angew. Chem. Int. Ed*., 2011, **50**, 6799.

32 J. Hafizovic, M. Bjørgen, U. Olsbye, P. D. C. Dietzel, S. Bordiga, C. Prestipino, C. Lamberti and K. P. Lillerud, *J. Am. Chem. Soc.*, 2007, **129**, 3612-3620.

33 C. Serre, C. M. Draznieks, S. Surblé, N. Audebrand, Y. Filinchuk and G. Férey, *Science*., 2007, **315**, 1828.

34 T. Teranishi and M. Miyake, *Chem. Mater.*, 1998, **10**, 594.

35 Y. Pan, B. Yuan, Y. Li and D. He, *Chem. Commun*., 2010, **46**, 2280.

36 F. Schro¨der, D. Esken, M. Cokoja, M. W. E. van den Berg,O. I. Lebedev, G. V. Tendeloo, B. Walaszek, G. Buntkowsky, H.-H. Limbach, B. Chaudret and R. A. Fischer, *J. Am. Chem. Soc*.,2008, **130**, 6119–6130.

37 F. Ke, J. Zhu, L-G Qiu and X. Jiang, *Chem. Commun*., 2013, **49**, 1267-1269.

38 S. Dutta, S. Sarkar, C. Ray, A. Roy, R. Sahoo, and T. Pal, *ACS Appl. Mater. Interfaces*, 2014, **6**, 9134.

39 H. L. Jiang, T. Akita, T. Ishida, M. Haruta, and Q. Xu, *J. Am. Chem. Soc*. 2011, **133**, 1304.

40 Y. Wu, M. Wen, Q. S. Wu and H. Fang, *J. Phys. Chem. C,* 2014, **118**, 6307.

Centre for Soft Matters, Department of Chemistry, Assam University, Silchar-788011, Assam, India. E-mail: himadriau@yahoo.co.uk Fax: +91 3842 270802; Tel: +91 3842 270848

